Observation of Energy Gain at the BNL Inverse Free-Electron-Laser Accelerator

A. van Steenbergen,[1,*] J. Gallardo,[1,†] J. Sandweiss,[2] and J.-M. Fang[3]
[1]*Brookhaven National Laboratory, Upton, New York 11973*
[2]*Physics Department, Yale University, New Haven, Connecticut 06511*
[3]*Department of Applied Physics, Columbia University, New York, New York 10027*
(Received 29 April 1996)

A 40 MeV electron beam, using the inverse free-electron-laser interaction, has been accelerated by $\Delta E/E = 2.5\%$ over a distance of 0.47 m. The electrons interact with a 1–2 GW CO_2 laser beam bounded by a 2.8 mm i.d. sapphire circular waveguide in the presence of a tapered wiggler with $B_{\max} \approx 1$ T, and a period $2.89 \leq \lambda_w \leq 3.14$ cm. The experimental results of $\Delta E/E$ as a function of electron energy E, peak magnetic field B_w, and laser power W_l compare well with analytical and 1D numerical simulations and permit scaling to higher laser power and electron energy. [S0031-9007(96)01273-2]

PACS numbers: 41.75.Lx, 41.60.Cr, 41.75.Ht, 52.75.Ms

Since the inception of practicable lasers, laser-driven acceleration concepts have been intensively studied. The interest resides in the use of the very large electric fields achievable by focusing the laser to very small spots. These fields are well in excess of the accelerating gradients currently obtained in rf cavities. The study of the inverse free-electron laser (IFEL) as a potential mode of electron acceleration has been pursued at Brookhaven National Laboratory (BNL) for a number of years [1–4]. Although the concept has been studied theoretically in detail, the first experimental verification of the concept ($\lambda = 1.65$ mm) was performed in 1992 [5]. In this Letter further experimental evidence of the IFEL interaction ($\lambda = 10.6$ μm) is presented. The experiment used a 50 MeV electron beam, a 1–5 GW CO_2 laser beam provided by the BNL's Accelerator Test Facility (ATF) and a uniquely designed period length tapered wiggler.

This wiggler is a fast excitation electromagnet with stackable, geometrically and magnetically alternating substacks of vanadium permendur (VaP) ferromagnetic laminations, periodically interspersed with conductive (Cu), nonmagnetic laminations, which act as eddy current induced field reflectors [6,7]. Four current conducting rods, parallel to the wiggler axis, are connected at the ends of the assembly, constituting the excitation loop that drives the wiggler. The overall wiggler stack is easily assembled, is compressed by simple tie rods, and readily permits wiggler period length (λ_w) variation. Configured as a constant period wiggler, $\lambda_w = 3.75$ cm and $B_{\max} = 1$ T, the system has shown [7] an rms pole-to-pole field variation of approximately 0.2%.

The CO_2 laser beam is brought into the IFEL interaction region by a low loss dielectric (sapphire) circular waveguide. Two different guide configurations were tested, first a $\frac{1}{4}$ λ dielectric coating (germanium) deposited on the two lateral walls of a rectangular cross-section metallic waveguide [8] and then a sapphire (Al_2O_3) circular waveguide, which showed very good transmission properties [9] of a high power CO_2 laser beam. Extensive studies were carried out to establish optimum coupling into the guide and to measure the transmission loss of long (1.0 m) extruded single crystal sapphire guides. Also, because of the overmoded guide configuration (i.d. = 2.8 mm), attempts were made to determine the transverse mode spectrum. To this end various waveguide configurations were tested at low laser beam power with the beam focused to a Gaussian waist with adjustable radius at the entrance of the waveguide. The beam profile was measured using a pyroelectric vidicon TV camera combined with digital frame grabber. For the circular sapphire dielectric guide a laser power attenuation factor of 0.2 dB/m was measured. The laser beam profile within the guide was inferred by measuring the beam diameter at the guide exit for various guide lengths. The results show that, commensurate with the near constant beam profile within the guide, the mode structure is dominated by the guide fundamental mode only. This is in accord with the absence of mode mixing reported in Ref. [9] for filamentary sapphire guides for CO_2 laser transport.

The laser power must be efficiently coupled into the desired mode (HE_{11}). To determine the transition region over which the mode becomes established, a series of scalar diffraction calculations were performed to find the fields propagating from the coupling aperture. It was found that the mode pattern transformed from the input

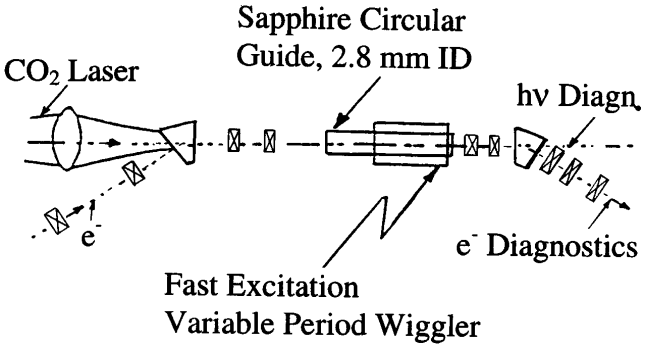

FIG. 1. Schematic of the experimental configuration.

 0031-9007/96/77(13)/2690(4)$10.00

Gaussian to a stable field distribution over a distance comparable to Z_R, the Rayleigh length. For the waist sizes employed here, after the mode has stabilized, the amplitude typically fluctuates by $\pm 5\%$ and the phase by ± 0.05 rad. These calculations suggest a 90% coupling efficiency into the desired mode, consistent with the experimental observations reported below.

In the IFEL accelerator, the electron beam is accelerated by the interaction with the laser radiation wave in the medium of a periodic wiggler field. The theoretical description of the interaction has been given by a number of authors [2,10]. Approximate analytical expressions derived in Ref. [2] were used to parametrize a single acceleration stage. Subsequently, 1D and 3D simulation programs were written solving the self-consistent system of Lorentz equations for the electrons and the wave equations for the input laser field as discussed in Ref. [10]. The 1D program has been used to determine the self-consistent wiggler period length and its taper for given values of electron beam energy and laser power and to calculate the bucket acceptance and bucket leakage for a single- or multimodule accelerator.

Extensive IFEL simulation studies were carried out both for a single IFEL accelerator module and for a sequence of IFEL modules. The objective of the present experiment was a proof of principle performance of a single IFEL unit incorporated in beam line II of the ATF. A schematic layout is shown in Fig. 1. Beam transport downstream from the nominal 50 MeV linac is so dimensioned as to yield a dispersion free IFEL interaction region. The electron beam, at the IFEL location, is matched vertically to the natural wiggler betatron amplitude $\beta_y = 0.17$ m, $\alpha_y = 0.0$ and to a horizontal amplitude $\beta_x = 0.3$ m, $\alpha_x = 0.0$. Downstream of the IFEL interaction region the optical system is configured as a momentum spectrometer with adjustable dispersion magnitude ($0.0 < \eta_p < 3.0$ m) at a diagnostic endstation; there the beam momentum dispersion is measured by means of a phosphor screen-vidicon TV camera-Spiracon frame grabber. Also shown schematically in Fig. 1 is the CO_2 laser beam entry into the interaction region vacuum envelope through a ZnSe window, and its propagation as a free-space mode, to the sapphire dielectric waveguide entry. With deliberation, the dielectric guide was taken to be 0.6 m in length, whereas the accelerator module length (wiggler length) was set at 0.47 m. This was done to approximate a mode matching section, enhancing thereby the mode purity in the IFEL module proper.

The design parameters used in this IFEL accelerator experiment are listed in Table I. With optimized overlap of the electron and CO_2 laser beams, both spatially and timewise, and the interleaving of the lower repetition rate CO_2 laser pulses with the higher repetition rate electron beam pulses, the IFEL electron beam acceleration could readily be established. Electron acceleration was measured with the spectrometer at the diagnostic screen. An example of the momentum spectrum of the unaccelerated and accelerated electrons is given in Fig. 2, where the beam intensity distribution is shown versus $\sqrt{\beta_x \epsilon_x} + \eta_p(\Delta p/p)$, with the spectrometer optics adjusted so that $\eta_p(\Delta p/p) \gg \sqrt{\beta_x \epsilon_x}$. Optimization of the IFEL effect and exploration of parameter space, with variation of the electron beam injection energy, CO_2 laser power, and wiggler maximum magnetic field magnitude was carried out in several consecutive runs, establishing the unambiguous signature of the IFEL acceleration. This is illustrated in Figs. 3, 4, and 5 where $(\Delta E/E)_{\mathrm{IFEL}}$ is shown both as given by the 1D model simulations and as obtained experimentally. Figure 3 shows the relative energy gain for B_w and W_l constant; in Fig. 4 the plot of $(\Delta E/E)_{\mathrm{IFEL}}$ vs B_w is given and in Fig. 5 the relative energy gain versus the laser power W_l is plotted. Although not shown in the figures, a maximum of $\Delta E/E = 2.5\%$ was measured with $E = 40$ MeV, $B_w = 1$ T, and $W_l = 1$ GW.

The approximate IFEL design equations [2] are

$$\frac{d\gamma}{dz} = \frac{AKf(K)}{\gamma} \sin\Psi \quad \text{where } \Psi = (k + k_w)z - kct, \tag{1}$$

where the normalized laser electric field is $A = (e/mc^2) \times (\pi W_l Z_0)^{1/2}/R_0$, $K = eB_w\lambda_w/2\pi mc \approx 2.7$ is the wiggler parameter, $f(K) \approx 0.38$ is a correction factor due to the linear polarization of the wiggler, $Z_0 = 377\ \Omega$ and k, k_w

TABLE I. Design parameters of the IFEL accelerator.

Electron beam	
Injection energy (MeV)	40.0
Exit energy (MeV)	42.3
Mean accelerator field (MV/m)	4.9
Current, nominal (mA)	5
N (bunch)	10^9
$I_{\max}$ (A)	30
$\Delta E/E(1\sigma)$	$\pm 3 \times 10^{-3}$
rms emittance (m rad)	7×10^{-8}
Beam radius (mm)	0.3
Wiggler	
L_w (m)	0.47
Section length (m)	0.6
Period λ_w (cm)	2.89–3.14
Gap (mm)	4
$B_w^{\max}$ (T)	1.0–1.024
Beam oscillation $a_{1/2}$ (mm)	0.16–0.19
Laser beam	
Power W_l (GW)	1
Wavelength λ (μm)	10.6
Maximum field E_0 (MV/m)[a]	0.78×10^3
Guide loss α (m^{-1})	0.05
Field attenuation (dB/section)	0.26
τ, FWHM (ps)	200–300
Normal field A (m^{-1})	1.53×10^3
Beam waist $r_0(L_w/2)$ (mm)	1.0

[a] $E_0 = (\pi W_l Z_0)^{1/2}/R_0$, $Z_0 = 377\ \Omega$, and $R_0 = 2.8$ mm waveguide radius.

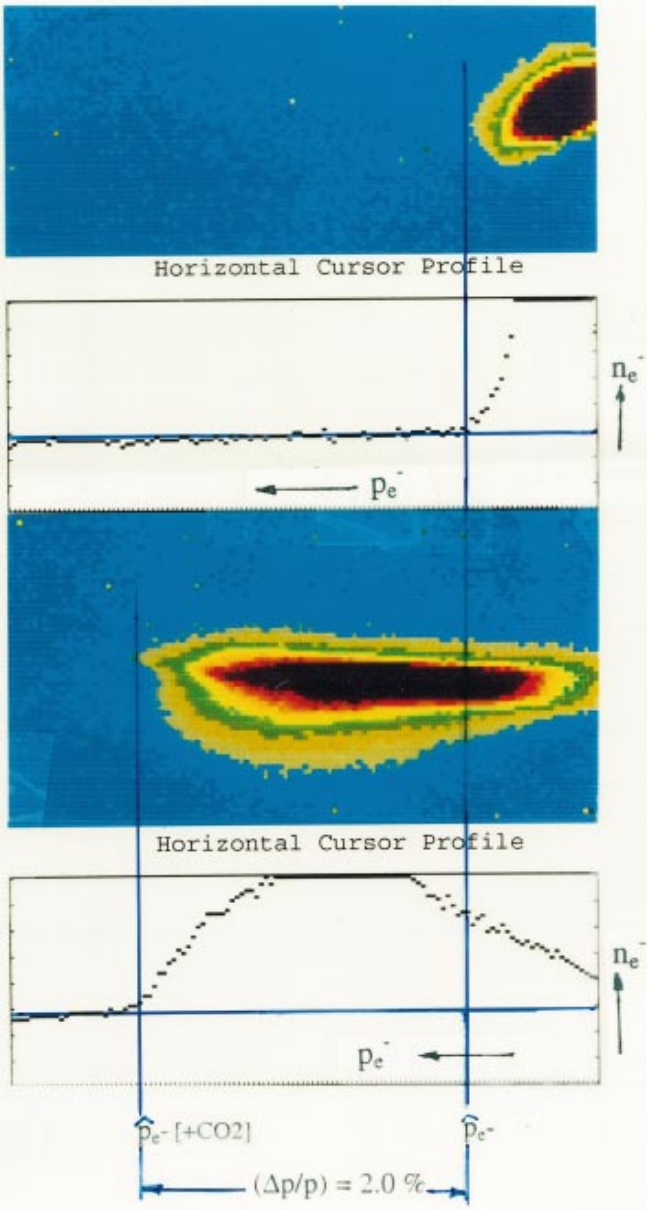

FIG. 2(color). Momentum spectrum of the unaccelerated and IFEL accelerated electron beam. E (linac) = 40 MeV, B_w = 10 kG, λ_w = 2.9−3.1 cm, W_l = 1 GW.

are the radiation and wiggler wave vectors, respectively. The resonance condition leads to

$$\lambda = (\lambda_w/2\gamma^2)(1 + K^2/2). \quad (2)$$

The relative energy gain of the electron beam in a wiggler of length L_w is

$$\frac{\Delta\gamma}{\gamma} = \left(\frac{\Delta p}{p}\right)_{\text{IFEL}} = \frac{AKf(K)}{\gamma^2} \sin\Psi_r L_w . \quad (3)$$

Here Ψ_r is the resonance phase (45° for optimum bucket size).

In Fig. 3 the solid line shows the results of the numerical simulations with laser power W_l = 1 GW and B_w = 10 kG normalized to the maximum experimental value. The agreement of the simulations with the experimental results are good. Similarly, in Fig. 4 experimental results are compared with the simulations for 35 and 40 MeV; in both cases the agreement is good. The maximum $(\Delta p/p)_{\text{IFEL}}$ for initial electron energy of 35 MeV leads to a value of the magnetic field B_w = 8.35 kG, to be compared with the experimental value of 8.44 kG, and for E = 40 MeV, the calculated B_w is 9.98 kG and the experimental value was B_w = 9.96 kG.

Figure 5 shows the relative energy gain as a function of the square root of the laser power; the scattering of data points reflect the typical laser power pulse to pulse variation; as a consequence, every set of experimental

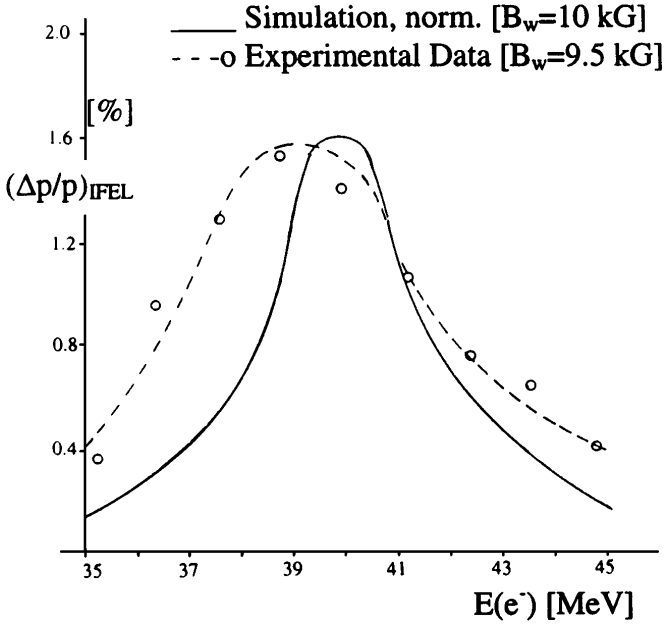

FIG. 3. Relative energy gain $\Delta E/E$ vs E with B_w, W_l constant.

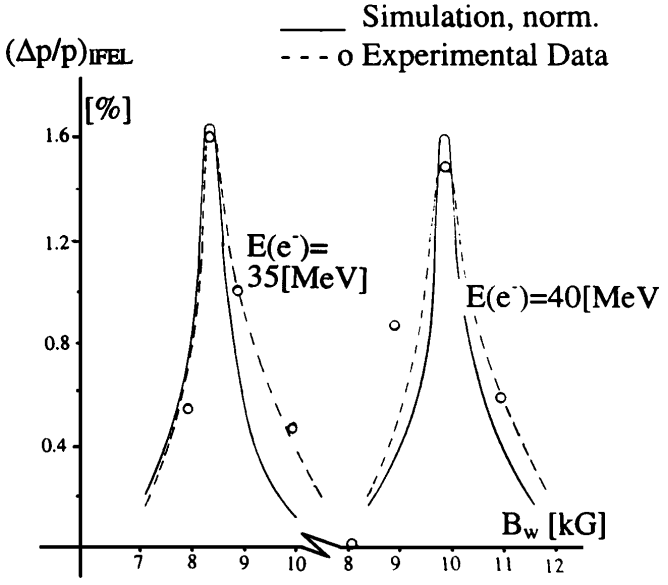

FIG. 4. Relative energy gain vs B_w with E and W_l constant.

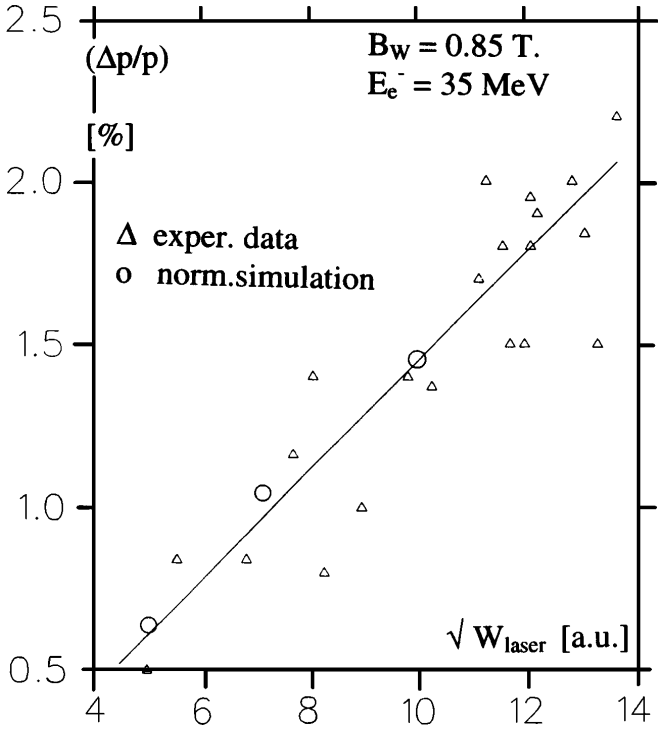

FIG. 5. Relative energy gain vs W_l with E and B_w constant.

data needs to be normalized to $\sqrt{W_l}$. With the present spectrometer, the energy gain could be measured with good accuracy due to the sharp intensity falloff of the high energy edge of the nonaccelerated particles. A quantitative intensity ratio of accelerated to unaccelerated beam could not be obtained due to the extended low energy edge of the unaccelerated beam. This limited the ability to measure the bucket size and leakage for comparison with model predictions and therefore, the value of the synchronous phase angle Ψ_r could not be unambiguously established. Analytically, Ψ_r and $\Delta\gamma/\gamma$ as function of laser power W_l and wiggler parameters are given by

$$\sin\psi_r = \frac{3}{16}\left(\frac{k}{k_w}\right)\frac{K}{Af(K)L_w}\left\{\left(\frac{\lambda_w(L)}{\lambda_w(0)}\right)^2 - 1\right\},$$
$$\frac{\Delta\gamma}{\gamma} = 2\sqrt{\frac{Kf(K)A}{k(1+K^2/2)}}\,\Gamma(\Psi_r)\,. \tag{4}$$

Equation (4) permits one to calculate the moving bucket [10] parameter $\Gamma(\Psi_r)$ and its maximum energy extent $\Delta\gamma/\gamma$. For the experimental value $(\Delta\gamma/\gamma)_{\mathrm{IFEL}} = 2.5\%$, we find $\Psi_r = 34°$ in reasonable agreement with the optimal 45° and a laser power of $W_l = 2.7$ GW which is larger than 1 GW estimated experimentally.

In conclusion, the IFEL acceleration of a 40 MeV electron beam by $\Delta E/E = 2.5\%$ with a 1 GW CO_2 laser and a tapered wiggler with peak field on axis of 10 kG has been confirmed. Agreement with the model predictions is satisfactory, permitting the scaling of anticipated results to higher laser power.

Present IFEL operation is limited to a maximum laser power of $\leq$2 GW. With enhanced vacuum pump-out capability of the IFEL interaction region and shorter laser pulse, operation at a laser power of 5 GW is planned which would enable close to 10% energy gain. With the upgrading of the ATF CO_2 laser to the 1 TW level as presently underway, the IFEL acceleration gradient of 100 MeV/m might become achievable. On this regards, limitations on energy gain may arise from at least two sources [11]: first, the damage threshold of the sapphire waveguide and the consequent potential decrease of the power transmission; second, the decrease of the electron beam intensity associated with self-field interaction due to the small aperture of the guide. These problems will be addressed in our next experimental runs.

The authors acknowledge the invaluable support of the ATF staff, in particular, M. Babzien, K. Batchelor, I. Ben-Zvi, A. Fisher, K. Kusche, R. Malone, I. Pogorelsky, J. Qiu, T. Romano, J. Sheehan, J. Skaritka, T. Srinivasan-Rao, and X.-J. Wang. This work was supported by the Advanced Technology R&D Branch, Division of High Energy Physics, U.S. Department of Energy, DE-AC02-76CH00016.

*National Synchrotron Light Source.
†Physics Department, 901-A. To whom correspondence should be addressed.
Electronic address: gallardo@bnl.gov

[1] R. Palmer, J. Appl. Phys. **43**, 3014 (1972).
[2] E. Courant, C. Pellegrini, and W. Zakowicz, Phys. Rev. A **32**, 2813 (1985).
[3] A. Fisher, J. Gallardo, J. Sandweiss, and A. van Steenbergen, in *Advanced Accelerator Concepts*, edited by J. S. Wurtele, AIP Conf. Proc. No. 279 (AIP, New York, 1993).
[4] A. Fisher, J. Gallardo, A. van Steenbergen, and J. Sandweiss, Nucl. Instrum. Methods Phys. Res., Sect. A **341**, ABS 111 (1994).
[5] I. Wernick and T. C. Marshall, Phys. Rev. A **46**, 3566 (1992).
[6] A. van Steenbergen, Patent No. 4,949,344 (1990).
[7] A. van Steenbergen, J. Gallardo, T. Romano, and M. Woodle, in *Fast Excitation Variable Period Wiggler, Proceedings of the PAC, San Francisco* (IEEE, New York, 1991); A. Fisher, J. Gallardo, A. van Steenbergen, J. Sandweiss, and J.-M. Fang, *Inverse Free Electron Laser Development, VI Workshop on Advanced Accelerators, Fontana, WI, 1994* (AIP Press, Woodbury, New York, 1995).
[8] W. Zakowicz, J. Appl. Phys. **55**, 3421 (1984).
[9] J. Harrington and C. Gregory, Opt. Lett. **15**, 6 (1990).
[10] N. Kroll, P. Morton, and M. Rosenbluth, Phys. Quantum Electron. **7**, 89 (1979).
[11] P. Sprangle, E. Esarey, and J. Krall, Phys. Plasmas **3**, 2183 (1996).